

AN UPPER LIMIT ON ANOMALOUS DUST EMISSION AT 31 GHz IN THE DIFFUSE CLOUD
[LPH96]201.663+1.643

C. DICKINSON¹, S. CASASSUS², J. L. PINEDA^{2,3}, T. J. PEARSON¹, A. C. S. READHEAD¹ AND
R. D. DAVIES⁴
Draft version September 26, 2018

ABSTRACT

[LPH96]201.663+1.643, a diffuse HII region, has been reported to be a candidate for emission from rapidly spinning dust grains. Here we present Cosmic Background Imager (CBI) observations at 26 – 36 GHz that show no evidence for significant anomalous emission. The spectral index within the CBI band, and between CBI and Effelsberg data at 1.4/2.7 GHz, is consistent with optically thin free-free emission. The best-fitting temperature spectral index from 2.7 to 31 GHz, $\beta = -2.06 \pm 0.03$, is close to the theoretical value, $\beta = -2.12$ for $T_e = 9100$ K. We place an upper limit of 24% (2σ) for excess emission at 31 GHz as seen in a 6' FWHM beam. Current spinning dust models are not a good fit to the spectrum of LPH96. No polarized emission is detected in the CBI data with an upper limit of 2% on the polarization fraction.

Subject headings: radio continuum: ISM — ISM: individual (LPH96) — radiation mechanisms: general — dust, extinction — polarization

1. INTRODUCTION

To extract precise cosmological information from high-sensitivity cosmic microwave background (CMB) data, the Galactic foregrounds must be accurately known over a wide frequency range. Galactic radiation, which comprises 3 well-known components (synchrotron, free-free and vibrational dust), is the most important on angular scales $\gtrsim 1^\circ$. However, many authors have detected an additional “anomalous” component in the frequency range $\sim 10 - 60$ GHz whose origin is still not understood. The anomalous emission, first detected in the COBE-DMR maps at 31- and 53-GHz, was initially thought to be due to free-free emission owing to its correlation with FIR maps and its spectral index (Kogut et al. 1996a,b). It soon became clear that free-free emission could not account for this “excess” due to the lack of H α emission. Observations of the NCP region at 14.5- and 32-GHz (Leitch et al. 1997) clearly show the anomalous emission and the tight correlation with 100 μ m maps. Since then, anomalous emission has been detected by a number of authors (de Oliveira-Costa et al. 2002, 2004; Banday et al. 2003; Lagache 2003; Finkbeiner 2004; Finkbeiner et al. 2004; Casassus et al. 2004; Watson et al. 2005; Davies et al. 2006) but still little is known about the physical mechanism that produces it. Candidates include spinning dust grains (Draine & Lazarian 1998a,b), magnetic dust emission (Draine & Lazarian 1999), flat-spectrum synchrotron (Bennett et al. 2003b) and free-free emission from very hot electrons (Leitch et al. 1997).

The first targeted search for spinning dust emission from individual objects was carried out by Finkbeiner et al. (2002). Using the Green Bank 140ft telescope, with a resolution of 6', they made scans of 10 dust clouds to look for the spectral signature of spinning dust grains i.e. a sharp rise from low frequencies up to a peak at ~ 20 GHz. They

saw a rise in the flux density over the frequency range 5 – 10 GHz for 2 objects: [LPH96]201.663+1.643 (henceforth LPH96) and LDN1622, both strongly correlated with FIR maps. The spectrum of LDN1622 appears to fit a spinning dust model remarkably well, a result that has recently been confirmed with CBI data at 31 GHz (Casassus et al. 2006). LPH96 is the brighter of the two clouds and is classed as a diffuse HII region (Lockman et al. 1996).

In §2 we present CBI total intensity and polarization observations of LPH96 in the range 26 – 36 GHz. The mapping capability of CBI provides an angular resolution $\sim 6'$ (similar to Green Bank observations). In §3 we compare low frequency radio maps at 1.4 and 2.7 GHz with CBI data at 31 GHz, both in the image and Fourier planes. §4 discusses the Green Bank data of Finkbeiner et al. (2002) and the correlations with the 100 μ m dust template. Discussion and conclusions are given in §5.

2. CBI DATA

The Cosmic Background Imager (CBI) is a 13-element interferometer situated on the high altitude Chajnantor site in Chile. In a compact configuration, baseline lengths range from 1.0m to 4.0m corresponding to angular scales between $\sim 6'$ and $\sim 30'$. The CBI covers the frequency range 26 – 36 GHz in 10 1 GHz channels. Observations of LPH96 (RA(J2000)=06:36:40, DEC(J2000)=+10:46:28) were taken on the nights of 15,17 and 19 November 2002 with a combined integration time of ~ 3000 s. Each receiver measures either left (L) or right (R) circular polarization, thus each baseline measures either total intensity (LL or RR) or polarization (LR or RL), which are combined in the u, v -plane to give Stokes I, Q, U . We assume that circular polarization, $V = 0$. A longer integration of ~ 3600 s was made in total intensity mode (all receivers measuring L only) on 14 January 2003.

¹ Dept. of Astronomy, California Institute of Technology, M/S 105-24, Pasadena, CA 91125, U.S.A.

² Departamento de Astronomía, Universidad de Chile, Casilla 36-D, Santiago, Chile.

³ Argelander-Institut für Astronomie, Universität Bonn, Auf dem Hügel 71, D-53121, Bonn, Germany.

⁴ Jodrell Bank Observatory, University of Manchester, Lower Withington, Macclesfield, Cheshire, SK11 9DL, U.K.

The data were reduced using similar routines to those used for CMB data (Pearson et al. 2003; Readhead et al. 2004a,b). Each 8-min integration on source was accompanied by a trail field, separated by 8 mins in RA, observed at the same hour angle for subtraction of ground-spillover. The overall absolute calibration scale is tied to a Jupiter temperature of $T_J = (147.3 \pm 1.8)$ K (Readhead et al. 2004a). Secondary calibrators (Tau-A, Jupiter, 3C274) were used to estimate a further uncertainty of $\sim 2\%$ in the gains on a given night. We therefore assign a total calibration uncertainty of 3%.

The final CBI CLEANed total intensity map is shown in Fig. 1. The excellent u, v coverage provides robust mapping of both compact and extended emission on scales up to $\sim 30'$ within the primary beam of $45'.2$ FWHM at 31 GHz. The peak flux density at 31 GHz is 1.79 Jy/beam centered on LPH96 but with some extended emission, mainly to the NW with a deconvolved angular size of $\sim 20'$. The noise level is ≈ 10 mJy/beam. Low level extended emission is also detected outside the FWHM of the primary beam, particularly to the SE of LPH96. Two elliptical Gaussians can account for the majority of the flux in the CLEANed map with an integrated flux density (after correcting for the primary beam) of 7.57 ± 0.4 Jy and residual rms of ≈ 30 mJy. The 2 components are 4.1 Jy centered on the peak of LPH96 with a deconvolved angular size of $9'.7 \times 6'.3$ and an extended component with angular size $20'.2 \times 17'.0$ containing 3.5 Jy. By splitting the bands into low and high frequencies, maps at 28.5 and 33.5 GHz were produced. However, due to the different u, v coverage, the maps have different resolution and spatial scales making it difficult to compare the flux densities of extended sources. Nonetheless, the peak flux density in a restored $6'$ FWHM beam was 1.75 and 1.71 Jy/beam at 28.5 and 33.5 GHz, respectively. This implies a flux spectral index⁵ $\alpha = -0.14 \pm 0.19$ over this range.

The polarization mapping capability of the CBI has been demonstrated from deep CMB observations (Cartwright et al. 2005; Readhead et al. 2004b; Sievers et al. 2005). The Stokes Q and U images of LPH96 have a r.m.s. noise level of ~ 14 mJy/beam, with a synthesized beam of $7'.9 \times 6'.5$ (FWHM). No significant polarization is detected above the noise from this region on these angular scales. From the noise-corrected polarization intensity map we place a 3σ upper limit on the polarization intensity of 34 mJy. This corresponds to a polarization fraction upper limit of 2% of the peak. For the extended emission to the NW, with a brightness of ~ 0.2 Jy/beam, the upper limit increases to $\approx 10\%$.

3. COMPARISON WITH LOW FREQUENCY RADIO MAPS

At lower frequencies, the all-sky surveys at 408 MHz (Haslam et al. 1982), 1420 MHz (Reich & Reich 1986) and 2326 MHz (Jonas et al. 1998) do not have sufficient angular resolutions ($51'$, $35'$ and $20'$ FWHM, respectively) to allow a reliable comparison with CBI data. Instead we use data from the Effelsberg 100-m telescope at 1408 MHz (Reich et al. 1997) and 2695 MHz (Fürst et al. 1990). The data⁶ are fully-sampled background subtracted continuum maps with beams of FWHM $9'.4$ and $4'.3$ respectively.

⁵ The temperature spectral index β is related to the flux density spectral index α by $\beta = \alpha - 2$ in the Rayleigh-Jeans limit.

⁶ The Effelsberg survey data were downloaded from the MPIfR sampler survey website: <http://www.mpifr-bonn.mpg.de/survey.html>

The 1.4 GHz map has a peak brightness temperature $T_b = 6.88$ K and LPH96 is almost unresolved (Fig. 2a). The 2.7 GHz map (Fig. 2b) has a peak $T_b = 3.38$ K and shows the extension to the NW detected in the CBI image. After smoothing to a common resolution of $9'.4$, the peak brightness at 2.7 GHz is $T_b = 1.86$ K, which corresponds to a temperature spectral index $\beta_{1.4}^{2.7} = -2.02 \pm 0.11$ (we assume a calibration uncertainty of 5% in the Effelsberg data).

To allow a comparison with CBI data, the 2.7 GHz map is “observed” with the CBI u, v coverage. This involves sampling the fourier transform of the 2.7 GHz map after multiplying the image by the CBI primary beam (and also making a correction for the smoothing due to the Effelsberg beam). The CLEANed image of the 2.7 GHz simulated map is shown as contours in Fig. 2b. The image is a good match to the CBI map with a peak flux density of 2.06 ± 0.10 Jy/beam and an integrated flux density for the LPH96 region of 7.6 ± 0.4 Jy. The peak flux densities at 2.7 and 31 GHz in the CBI beam correspond to a flux density spectral index $\alpha = -0.06 \pm 0.03$.

We also compare data in the Fourier plane by simulating the CBI observation given an input map (as in the image analysis), but comparing the visibilities directly. This allows direct comparison of CBI data with multi-frequency maps without the problems of deconvolution and incomplete u, v coverage. The noise in each visibility can be treated as independent so we can simply compute the slope of the best-fitting linear relationship between the visibilities at the two frequencies. The Pearson’s correlation coefficient, $P = 0.93$, indicates a strong correlation between CBI data and the 2.7 GHz map. The fitted slopes from 31 GHz to 1.4 and 2.7 GHz are 2.06 ± 0.12 mK/K and 7.13 ± 0.42 mK/K respectively. This corresponds to spectral indices of $\beta_{1.4}^{31} = -2.00 \pm 0.04$ and $\beta_{2.7}^{31} = -2.02 \pm 0.04$. The slopes for each CBI channel can be calculated in the same way, but are less useful since each frequency samples different regions of the u, v -plane. Nevertheless, for correlations with the 2.7 GHz data, we get $\beta = -2.19 \pm 0.14$ over the range 26 – 36 GHz, in agreement with the image analysis.

4. COMPARISON WITH GREEN BANK DATA AND FIR MAPS

The Green Bank data presented by Finkbeiner et al. (2002) consist of $48'$ long scans at 5.8, 25 and 9.75 GHz, smoothed to a resolution $6'$ FWHM. The scans were chopped at $12'$ and a smooth baseline subtracted to remove ground (sidelobe) and atmospheric contamination. This makes it difficult to obtain accurate flux densities for extended structures.

However, Finkbeiner et al. (2002) do find a tight correlation with the Schlegel et al. (1998) $100 \mu\text{m}$ dust map which can be used to estimate the flux density. If the emissivity is constant within a given region, this allows comparison of data with different resolutions and/or observing strategies. The temperature-corrected $100 \mu\text{m}$ dust map is shown in Fig. 2c with a peak brightness of 479 MJy/sr at $6'.1$ resolution. The averaged emissivities from Finkbeiner et al. (2002), referenced to the $100 \mu\text{m}$ map, are 2770.5 ± 13.8 , 1361.0 ± 48.0 and $1262.5 \pm 49.5 \mu\text{K}/(\text{MJy/sr})$ at 5, 8, 25

and 9.75 GHz, respectively. The Pearson's correlation was $P = 0.91$ indicating the overall similarity between the radio and 100 μm data. The dust map was scaled with these values and observed with the CBI beam. For a restored CLEAN beam of 6' (FWHM), the peak flux densities were 1.97 ± 0.23 , 2.64 ± 0.10 , 3.38 ± 0.14 Jy at 5, 8.25 and 9.75 GHz, respectively.

To test whether there is a significant variation in 100 μm -referenced emissivity between extended and compact emission (which would invalidate the comparison), the correlation coefficient was calculated within a restricted u, v -range corresponding to either small or large angular scales. The correlation coefficient at 31 GHz was $41.6 \pm 1.2 \mu\text{K}/(\text{MJy}/\text{sr})$ and did not change significantly ($\lesssim 5\%$) for angular scales between 6' and 30'. Joint cross-correlations with multiple maps were not attempted since the structure in the radio and FIR maps is similar and would not allow a reliable separation of components.

5. DISCUSSION AND CONCLUSIONS

To quantify the contribution of dust emission at GHz frequencies, the free-free emission must be accurately known. The analysis of Finkbeiner et al. (2002) relied on $\text{H}\alpha$ data to place limits on the amount of free-free radiation, which was found to be dominant at 5 GHz. However, the effects of dust extinction can clearly be seen in the $\text{H}\alpha$ map (Gaustad et al. 2001) shown in Fig. 2d. LPH96 is visible at a level of ~ 250 R. For optically thin emission at 2.7 GHz, and assuming a typical electron temperature of $T_e \sim 7000 - 10000$ K, the $\text{H}\alpha$ -to-free-free conversion is ≈ 1 mK/R (Dickinson et al. 2003). The measured electron temperature from radio recombination lines (RRL) is $T_e = 9100$ K (Shaver et al. 1983). This would predict 0.25 K of free-free emission based on $\text{H}\alpha$ intensities and would require an absorption factor of > 10 to match the radio flux density. Making predictions based on $\text{H}\alpha$ are therefore unreliable. Observations of RRLs provide a complementary and clean method of separating the free-free thermal emission, without the effects of dust absorption. Lockman et al. (1996) measure a $\text{H}126\alpha$ line temperature for LPH96 of $T_L = (24 \pm 2.6)$ mK at 9' resolution. Assuming optically thin emission in local thermodynamic equilibrium, for $T_e = 9100$ K, this would predict 4.9 ± 0.5 K of free-free emission at 1.4 GHz in a 9' beam. This implies that the radiation at 2.7 GHz remains optically thin down to at least 1.4 GHz, thus allowing reliable extrapolation from 2.7 GHz to higher frequencies. There is low-level extended emission to the SE of LPH96 that has a similar spectrum suggesting that the emission in this entire region is dominated by optically thin free-free emission. The WMAP data⁷ (Bennett et al. 2003a), smoothed to 1° resolution, have a spectral index $\alpha = -0.22 \pm 0.14$ over the range 20 – 40 GHz. A detailed comparison of WMAP data and CBI data is not attempted due to the mismatch of resolutions.

The spectrum of LPH96, in terms of the flux density within a 6' (FWHM) Gaussian beam centered on LPH96, is shown in Fig. 3; 1.98 ± 0.10 Jy at 2.7 GHz and 1.71 ± 0.05 Jy at 31 GHz. The Green Bank points

were estimated by calculating the flux density in the 6' CBI beam of the 100 μm map scaled by the factors as measured by Finkbeiner et al. (2002) (see §4). The gray shaded area shows the allowed range for the free-free model based on extrapolating from 2.7 GHz using $-0.02 < \alpha < -0.12$. The range is based on the flattest derived spectral index ($\alpha = -0.02$) and the theoretical value ($\alpha = -0.12$); the best-fitting value from the image analysis, $\alpha = -0.06 \pm 0.03$, is in the middle of this range. The 5 GHz point is close to the free-free model, but at 8 – 10 GHz, the Green Bank data show a significant excess that cannot be reconciled with the 2.7 and 31 GHz data points. A spinning dust model for the Warm Neutral Medium (Draine & Lazarian 1998b), scaled in amplitude to fit the Green Bank data, is depicted in Fig. 3. From this, one would expect to see considerable emission in the 26 – 36 GHz CBI band, well above the free-free emission, which is not seen. It is interesting to note that the Galactic plane survey of Langston et al. (2000) at 8.35 GHz (11'.167 beam) detected LPH96 with a peak flux density of 3.69 Jy and integrated flux density of 6.74 Jy. But no detection was made at 14.35 GHz (8' beam), with a detection limit of 2.5 Jy. Given the spectral rise observed from 5 – 10 GHz, one would expect ≈ 5 Jy at 14.35 GHz.

If the spectrum is indeed increasing from 5 to 10 GHz, then the lack of anomalous emission at CBI frequencies suggests that either i) current spinning dust models are not a good fit for this particular cloud or ii) the emission is due to another mechanism. McCullough & Chen (2002) have suggested that the rising spectrum could occur if there was a dense optically thick ultracompact HII region within the cloud, which would exhibit a rising spectrum ($\alpha \approx 2$) with a flux density in the range 1.6 – 4.4 Jy at 15 GHz. High resolution data are required to definitively rule out this model, but it is unlikely given the CBI flux density.⁸

From the image analysis, we can constrain the non-free-free contribution at 31 GHz by subtracting the free-free model based on the extrapolation of 2.7 GHz data. A spectral index $\alpha = 0.06 \pm 0.03$ accounts for essentially all the emission seen at 31 GHz and is close to the canonical value of $\alpha = -0.1$ for free-free emission at GHz frequencies. Adopting the theoretical value, $\alpha = -0.12$ for $T_e = 9100$ K, the predicted flux density at 31 GHz in a 6' beam becomes 1.48 ± 0.07 Jy. This leaves 0.23 ± 0.09 Jy, or 14% of the total 31 GHz flux density, that could be due to an additional anomalous component. At this level the dust emissivity would be $\approx 6 \mu\text{K}/(\text{MJy}/\text{sr})$, within the range observed at high latitudes (e.g. Banday et al. (2003)). It is therefore possible that there is a non-negligible anomalous dust component in this HII region that is not detected because of the much brighter thermal emission. Given the sensitivity to the assumed spectral index, we do not claim a significant detection of anomalous emission at 31 GHz. We place an upper limit 0.41 Jy (2σ) on the anomalous emission at 31 GHz in a 6' beam, which corresponds to 24% of the total flux density.

The lack of polarization seen in the CBI data are consistent with free-free emission. If 14% of the emission at

⁷ WMAP all-sky maps available from <http://lambda.gsfc.nasa.gov/>.

⁸ D. Finkbeiner et al. (priv. comm) have recently re-observed LPH96 using the 100m Green Bank Telescope (GBT) in the frequency range 5 – 18 GHz. They could not reproduce the rising spectrum as seen with the 140ft telescope.

31 GHz was indeed anomalous, then the polarization of this component is $\sim 10\%$ (2σ). This largely rules out emission from aligned grains of strongly magnetic material that is expected to be highly polarized (Draine & Lazarian 1999).

More data are required to clarify the origin(s) of the anomalous emission, both at high and low Galactic latitudes, and to investigate the conditions in which it occurs. For LPH96, data in the range 5 – 20 GHz are required to investigate further the anomalous emission reported by Finkbeiner et al. (2002). A detailed understanding of anomalous/spinning dust emission will be important for modeling and removal of CMB foregrounds at frequencies $\lesssim 100$ GHz, particularly if they exhibit significant polarization.

We gratefully acknowledge support from the Kavli Operating Institute and thank B. Rawn and S. Rawn Jr for their continuing support. We are also grateful for the support of M. and R. Linde, C. and S. Drinkward

and the provost, president, and PMA division chairman of the California Institute of Technology. The CBI was supported by NSF grants 9802989, 0098734 and 0206416. We acknowledge the use of the Legacy Archive for Microwave Background Data Analysis (LAMBDA). Support for LAMBDA is provided by the NASA Office of Space Science. We acknowledge the use of NASA's SkyView facility (<http://skyview.gsfc.nasa.gov>) located at NASA Goddard Space Flight Center. The Southern H-Alpha Sky Survey Atlas (SHASSA) is supported by the NSF. CD thanks Patricia Reich for maintaining the MPIfR image retrieval facility and making the Effelsberg data available. We thank Doug Finkbeiner for informing us of newGBT observations of LPH96. CD thanks Barbara and Stanley Rawn Jr for funding a fellowship at Caltech. SC acknowledges support from FONDECYT grant 1030805, and from the Chilean Center for Astrophysics FONDAF 15010003. JLP acknowledges the grant MECESUP UCH0118 given by the Chilean Ministry of Education.

REFERENCES

- Banday, A. J., Dickinson, C., Davies, R. D., Davis, R. J., & Górski, K. M. 2003, *MNRAS*, 345, 897
- Bennett, C. L., Halpern, M., Hinshaw, G., Jarosik, N., Kogut, A., Limon, M., Meyer, S. S., Page, L., Spergel, D. N., Tucker, G. S., Wollack, E., Wright, E. L., Barnes, C., Greason, M. R., Hill, R. S., Komatsu, E., Nolte, M. R., Odegard, N., Peiris, H. V., Verde, L., & Weiland, J. L. 2003a, *ApJS*, 148, 1
- Bennett, C. L., Hill, R. S., Hinshaw, G., Nolte, M. R., Odegard, N., Page, L., Spergel, D. N., Weiland, J. L., Wright, E. L., Halpern, M., Jarosik, N., Kogut, A., Limon, M., Meyer, S. S., Tucker, G. S., & Wollack, E. 2003b, *ApJS*, 148, 97
- Cartwright, J. K., Pearson, T. J., Readhead, A. C. S., Shepherd, M. C., Sievers, J. L., & Taylor, G. B. 2005, *ApJ*, 623, 11
- Casassus, S., Cabrera, G., Forster, F., Pearson, T. J., Readhead, A. C. S., & Dickinson, C. 2006, *ApJ*, accepted (astro-ph/0511283)
- Casassus, S., Readhead, A. C. S., Pearson, T. J., Nyman, L.-Å., Shepherd, M. C., & Bronfman, L. 2004, *ApJ*, 603, 599
- Davies, R. D., Dickinson, C., Banday, A. J., Jaffe, T. R., Gorski, K. M., & Davis, R. J. 2006, preprint (astro-ph/0511384)
- de Oliveira-Costa, A., Tegmark, M., Davies, R. D., Gutiérrez, C. M., Lasenby, A. N., Rebolo, R., & Watson, R. A. 2004, *ApJ*, 606, L89
- de Oliveira-Costa, A., Tegmark, M., Finkbeiner, D. P., Davies, R. D., Gutiérrez, C. M., Haffner, L. M., Jones, A. W., Lasenby, A. N., Rebolo, R., Reynolds, R. J., Tufte, S. L., & Watson, R. A. 2002, *ApJ*, 567, 363
- Dickinson, C., Davies, R. D., & Davis, R. J. 2003, *MNRAS*, 341, 369
- Draine, B. T. & Lazarian, A. 1998a, *ApJ*, 494, L19+
- . 1998b, *ApJ*, 508, 157
- . 1999, *ApJ*, 512, 740
- Finkbeiner, D. P. 2004, *ApJ*, 614, 186
- Finkbeiner, D. P., Langston, G. I., & Minter, A. H. 2004, *ApJ*, 617, 350
- Finkbeiner, D. P., Schlegel, D. J., Frank, C., & Heiles, C. 2002, *ApJ*, 566, 898
- Fürst, E., Reich, W., Reich, P., & Reif, K. 1990, *A&AS*, 85, 691
- Gaustad, J. E., McCullough, P. R., Rosing, W., & Van Buren, D. 2001, *PASP*, 113, 1326
- Kogut, A., Banday, A. J., Bennett, C. L., Gorski, K. M., Hinshaw, G., & Reach, W. T. 1996a, *ApJ*, 460, 1
- Kogut, A., Banday, A. J., Bennett, C. L., Gorski, K. M., Hinshaw, G., Smoot, G. F., & Wright, E. I. 1996b, *ApJ*, 464, L5+
- Lagache, G. 2003, *A&A*, 405, 813
- Langston, G., Minter, A., D'Addario, L., Eberhardt, K., Koski, K., & Zuber, J. 2000, *AJ*, 119, 2801
- Leitch, E. M., Readhead, A. C. S., Pearson, T. J., & Myers, S. T. 1997, *ApJ*, 486, L23+
- Lockman, F. J., Pisano, D. J., & Howard, G. J. 1996, *ApJ*, 472, 173
- McCullough, P. R. & Chen, R. R. 2002, *ApJ*, 566, L45
- Pearson, T. J., Mason, B. S., Readhead, A. C. S., Shepherd, M. C., Sievers, J. L., Udomprasert, P. S., Cartwright, J. K., Farmer, A. J., Padin, S., Myers, S. T., Bond, J. R., Contaldi, C. R., Pen, U.-L., Prunet, S., Pogogyan, D., Carlstrom, J. E., Kovac, J., Leitch, E. M., Pryke, C., Halverson, N. W., Holzzapfel, W. L., Altamirano, P., Bronfman, L., Casassus, S., May, J., & Joy, M. 2003, *ApJ*, 591, 556
- Readhead, A. C. S., Mason, B. S., Contaldi, C. R., Pearson, T. J., Bond, J. R., Myers, S. T., Padin, S., Sievers, J. L., Cartwright, J. K., Shepherd, M. C., Pogogyan, D., Prunet, S., Altamirano, P., Bustos, R., Bronfman, L., Casassus, S., Holzzapfel, W. L., May, J., Pen, U.-L., Torres, S., & Udomprasert, P. S. 2004a, *ApJ*, 609, 498
- Readhead, A. C. S., Myers, S. T., Pearson, T. J., Sievers, J. L., Mason, B. S., Contaldi, C. R., Bond, J. R., Bustos, R., Altamirano, P., Achermann, C., Bronfman, L., Carlstrom, J. E., Cartwright, J. K., Casassus, S., Dickinson, C., Holzzapfel, W. L., Kovac, J. M., Leitch, E. M., May, J., Padin, S., Pogogyan, D., Pospieszalski, M., Pryke, C., Reeves, R., Shepherd, M. C., & Torres, S. 2004b, *Science*, 306, 836
- Reich, P., Reich, W., & Furst, E. 1997, *A&AS*, 126, 413
- Schlegel, D. J., Finkbeiner, D. P., & Davis, M. 1998, *ApJ*, 500, 525
- Shaver, P. A., McGee, R. X., Newton, L. M., Danks, A. C., & Pottasch, S. R. 1983, *MNRAS*, 204, 53
- Sievers, J. L., Achermann, C., Bond, J. R., Bronfman, L., Bustos, R., Contaldi, C. R., Dickinson, C., Ferreira, P. G., Jones, M. E., Lewis, A. M., Mason, B. S., May, J., Myers, S. T., Padin, S., Pearson, T. J., Pospieszalski, M., Readhead, A. C. S., Reeves, R., Taylor, A. C., & Torres, S. 2005, *ApJ*, in press (astro-ph/0509203)
- Watson, R. A., Rebolo, R., Rubiño-Martín, J. A., Hildebrandt, S., Gutiérrez, C. M., Fernández-Cerezo, S., Hoyland, R. J., & Battistelli, E. S. 2005, *ApJ*, 624, L89

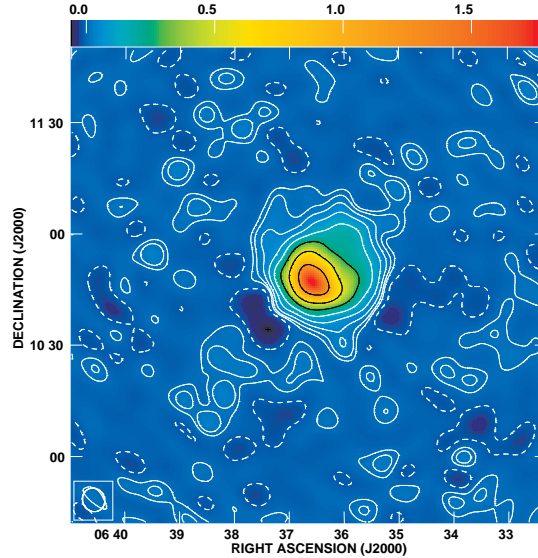


FIG. 1.— CBI 31 GHz total intensity CLEANed map of LPH96. The uniform weighted synthesized beam FWHM is $6'.5 \times 5'.9$. The primary beam ($45'.2$ FWHM) has not been corrected for in this image. Contours are at -0.5 (*dashed*), $0.5, 1, 2, 4, 8, 16, 32, 64\%$ of the peak flux density, 1.79 Jy/beam.

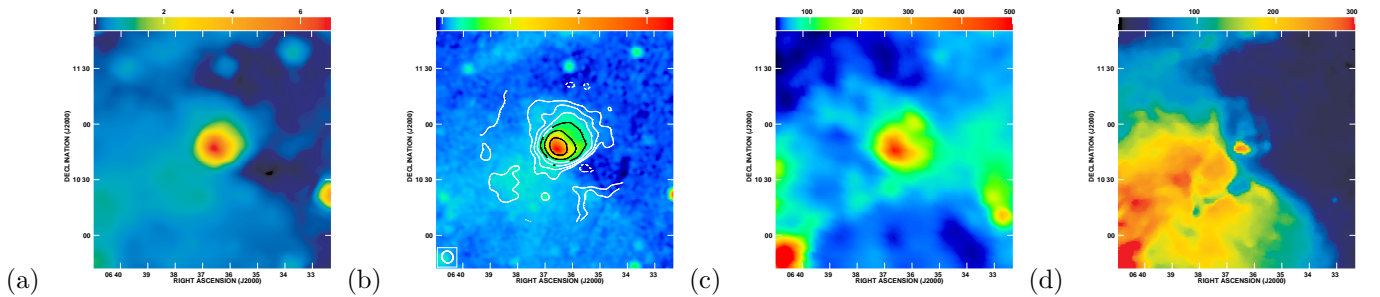


FIG. 2.— Multi-frequency maps of the LPH96 region, covering the same angular scale as Fig. 1, at their original resolutions (see text). (a) Effelsberg 21cm continuum map (units of K). (b) Effelsberg 2.7 GHz continuum map (units of K) overlaid with a CBI simulation of this data. The simulated map has been CLEANed and primary beam corrected down to 10% of the peak. Contours are at -2 (*dashed*), $2, 4, 8, 16, 32, 64\%$ of the peak intensity. (c) Schlegel et al. (1998) $100 \mu\text{m}$ temperature-corrected dust map (units of MJy/sr). (d) SHASSA continuum-subtracted $\text{H}\alpha$ map at $4'$ resolution (units of Rayleigh).

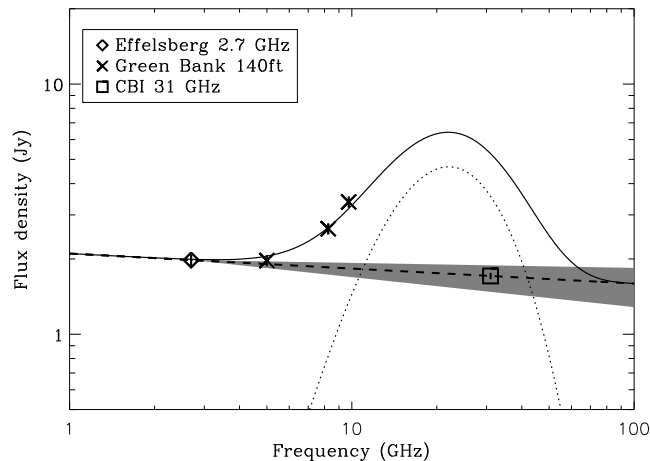


FIG. 3.— Spectrum of LPH96. Data points are in terms of the peak flux density in a $6'$ FWHM Gaussian beam, after being observed with the CBI beam. The Effelsberg 2.7 GHz point (*diamond*) is assumed to be due to free-free emission only. The dashed line is the emission extrapolated from 2.7 GHz with a flux density spectral index $\alpha = -2.06$. The shaded area represents the possible range for the free-free extrapolation from 2.7 GHz with $-0.12 < \alpha < -0.02$ (see text). The CBI flux density at 31 GHz (*square*) is seen to be dominated by free-free emission alone. The Green Bank 140 ft data, at 5, 8.25 and 9.75 GHz (*crosses*), are evaluated using correlations with the $100 \mu\text{m}$ dust template (see text). A spinning dust model for the Warm Neutral Medium (Draine & Lazarian 1998b), scaled to fit the Green Bank data, is shown as the *dotted line*. *Solid line* is the sum of free-free and spinning dust components.